Astron. & Astrophys. 14, 275–282 (1971)

On the Propagation of a Spectrum of Acoustic Waves in the Solar Atmosphere

PETER ULMSCHNEIDER
Astronomisches Institut und Sternwarte der Universität Würzburg

Received May 11, 1971

The propagation of acoustic waves, their transformation into shock waves and their dissipation has been computed on basis of the Harvard Smithsonian Reference Atmosphere (HRA) for the sun. Acoustic frequency spectra of Stein (1968) were used and the effect of radiative damping included. Good agreement was found between the heating produced by these waves and the computed radiative losses in the chromosphere. Coronal heating proved more difficult to explain.

Key words: acoustic waves — shock waves — chromosphere — corona

1. Introduction

In a previous paper (Ulmschneider, 1971) it was found that the frequency spectrum of the flux of acoustic waves produced in the convection zone of the sun determines very strongly the heating of different height levels in the chromosphere and corona.

Because high frequency waves develop into shock waves earlier the outer height levels are heated by successively lower frequency shock waves. In a qualitative way it could be stated that waves with periods of less than about 80 s are responsible for the heating of the chromosphere while waves of periods of 100 s or longer are the heating agents for the corona. Because of the lack of detailed computation including an adequate treatment of the radiative losses suffered by these waves this finding was of a qualitative nature only.

In this work an actual nonlinear computation including radiation effects is undertaken based on the frequency spectra of Stein (1968). Because the radiative losses were treated in an approximative manner taking account of the optical depth only in a very crude way it was decided that the mathematical treatment of the hydrodynamical equations need not to be carried to utmost accuracy. Instead of the explicit integration of the three differential equations integral principles were used. This proved to be entirely sufficient when compared with more detailed methods.

In Sec. 2 we describe this method of computation while Sec. 3 deals with the manner in which radiative losses are incorporated. The question of how to simulate the acoustic wavefield with its statistical nature on the computer is dealt with in Sec. 4. Sec. 5 gives results and a discussion.

Although this present work is only a step towards the detailed understanding of wave motion and heating processes in the outer solar atmosphere it may serve already as a means to assess the importance of acoustic waves for the generation of micro- and macroturbulence, and to get an idea of the influence of wave motion on the computation of empirical chromospheric models.

2. Method of Computation

The usual procedure to compute the propagation, profile growth and distortion of an acoustic wave is to integrate the hydrodynamic equations (e.g. Bird, 1964) by using either a finite difference scheme or the characteristics method. Although these methods appear conceptually to be quite simple they exhibit practical difficulties when they are applied to a problem where both soundvelocity, entropy and radiation loss are specified functions of height.

Moreover as radiative losses can only be treated very approximately it seems unnecessary to improve the accuracy in the mathematical treatment of the wave behavior while being very inaccurate in the dominant damping mechanism.

For this reason it was decided to use integral principles like the conservation of mechanical flux and the rate of profile distortion well known from the theory of simple waves. This proved to be surprisingly accurate in reproducing more detailed computations of Bird (1964). The radiation loss could

moreover easily be incorporated in the scheme as well as computation time greatly reduced.

Let us consider a periodic acoustic wave of small amplitude, that is, the velocity of the gas particles v is small against the sound velocity c. Then the energy flux carried by this wave may be written (Landau and Lifshitz, 1959, p. 250).

$$\pi F_{\text{Mech}} = \frac{1}{P}\int_0^P \varrho_0 v^2 c\, dt\,. \tag{1}$$

Here ϱ_0 is the density of the unperturbed atmosphere and P the period of the wave. Let us consider what happens to this flux.

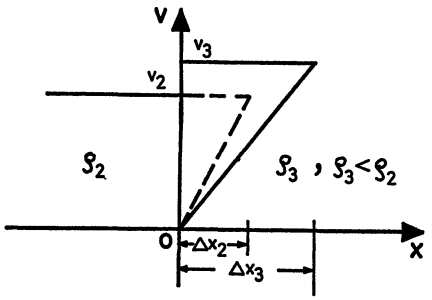

Fig. 1. Velocity v as a function of distance x for a rectangular shock wave moving through a density discontinuity at $x = 0$ is shown in presence (drawn) and absence (dashed) of the discontinuity

a) Conservation

For a wave of very small amplitude the profile essentially does not get distorted and is carried along with the sound velocity c. Let us assume that the sound wave is given for instance by a positive sinusoidal velocity pulse $v_1(i)$ of duration $P/2$ as shown e.g. in Fig. 3. This is taken to be representative for an infinite monochromatic sound wave of period P. Because the sound velocity changes along this pulse we cut it into I pieces of duration Δt and length $\Delta x = c\Delta t$ within which the sound velocity is considered constant. At the resulting height grid $x(i)$ which may be extended through the whole atmosphere we consider as given $c(i)$ and the density $\varrho_0(i)$ of the unperturbed atmosphere. The initial profil at time t_1 is thus given by

$$v_1(i), x_1(i)\,, \quad i = 1, \ldots, I+1 \tag{2}$$

After the time interval $K\Delta t$ where K is an integer, at the time

$$t_2 = t_1 + K\Delta t \tag{3}$$

the undistorted but steepened velocity profile $v_2'(i)$ may then be computed using Eq. (4)

$$\left.\begin{aligned} &\varrho_0(i+K)\, c(i+K)\, v_2'^2(i) \\ &\quad = \varrho_0(i)\, c(i)\, v_1^2(i) \\ &x_2(i) = x_1(i+K) \end{aligned}\right\} \; i = 1, \ldots I+1\,. \tag{4}$$

b) Profile Distortion

In cases where v is not very small against c the profile suffers a distortion well known from the theory of simple waves. Regions of high velocity travel faster than regions of low velocity such that the total velocity of a point in the profile is (Landau and Lifshitz, 1959, p. 368)

$$u = c + \frac{1}{2}(\gamma+1)\, v\,. \tag{5}$$

Here $\gamma = 5/3$ is the ratio of specific heats.

At the time t_2 the profile point $v_1(i)$ will be shifted by a height interval

$$\Delta x = \frac{1}{2}(\gamma+1)\, v(t_2 - t_1)\,, \tag{6}$$

where

$$v = \frac{(v_2'(i) + v_1(i))}{2} \tag{7}$$

to the height

$$x_2'(i) = x_2(i) + \Delta x\,. \tag{8}$$

Because we want the velocity profile at the old x spacing we interpolate in the $v_2'(i)$ versus $x_2'(i)$ table to obtain the distorted profile

$$v_2(i), x_2(i) \;\; i = 1, \ldots, I+1\,. \tag{9}$$

This was done using three point parabolas in $-v$ direction.

In a homogeneous atmosphere the process Eq. (6) to (9) ensures flux conservation as well. In a gravitational atmosphere the distorting shift must also be accompanied by a steepening. This may be seen most easily considering a rectangular shock wave at the interface between two constant density half-spaces (Fig. 1) labelled by suffixes 2 and 3. Let $\varrho_3 < \varrho_2$ and v_2 be the velocity of the shock front arriving at time $t = 0$ at the discontinuity $x = 0$. If no discontinuity were present the profile distortion at time t would be as indicated dashed. The amount

of energy lost at the high density side in the time interval Δt is thus

$$\Delta E_2 = \frac{2}{3} v_2^2 \varrho_2 \Delta x_2$$

$$\Delta x_2 = \frac{1}{2} (\gamma + 1) v_2 \Delta t$$

In reality we have a velocity discontinuity and the energy gained at the low density side is

$$\Delta E_3 = \frac{2}{3} v_3^2 \varrho_3 \Delta x_3$$

$$\Delta x_3 = \frac{1}{2} (\gamma + 1) v_3 \Delta t$$

Thus

$$\varrho_2 v_2^3 = \varrho_3 v_3^3 . \tag{10}$$

Using Eq. (10) we find for the final velocity profile at time t_2 under the action of both steepening and distortion

$$v_2'(i) = v_2'(i)\, e^{\frac{x_2'(i) - x_2(i)}{3H(i+K)}} \tag{11}$$

where

$$H(i+K) = \frac{c^2(i+K)}{\gamma g} \tag{12}$$

is the scale height at the height $x_2(i)$.

c) Formation of Shock Discontinuities

Eventually the above process Eqs. (4) to (12) will yield a multivalued curve

$$v_2'(i), x_2'(i) , \quad i = 1, \ldots I+1$$

and provision for the occurrence of a shock at the highest x points has to be taken. Because we assumed $v < c$ the resulting shock will be weak and thus travel with sound velocity. It will form exactly at the highest x point. Because the $x_2(i)$ is always smaller than $x_2'(i)$ three point interpolation parabolas in $-v$ direction are good for $i = 1, \ldots, I$. For the highest x point however we use an interpolation parabola going through $v_2'(I-1)$, $x_2'(I-1)$ and $v_2'(I)$, $x_2'(I)$ and $v_2'(I+1) = 0$, $x_2'(I+1)$ but opening toward $-x$ direction. We compute the second point of intersection of the parabola with the $x_2'(I+1) = \text{const.}$ axis by

$$v_s = \frac{v_2'(I)^2 (x_2'(I+1) - x_2'(I-1))}{v_2'(I)(x_2'(I+1) - x_2'(I-1))} \cdot \frac{- v_2'(I-1)^2 (x_2'(I+1) - x_2'(I))}{- v_2'(I-1)(x_2'(I+1) - x_2'(I))} \tag{13}$$

If $v_s > 0$ we have a shock discontinuity at $x_2(I+1)$ with velocity $v_2(I+1) = v_s$ else a node with $v_2(I+1) = 0$.

d) Comparison with Other Methods

This above method appears to be extremely stable and well behaved. It could easily be adapted to simulate the boundary value problem where the wave enters in time at a fixed x point. Using this boundary condition we simulated the somewhat different model computation of Bird (1964). A comparison of the height of shock formation with values given by Bird is shown in Table 1.

It is seen that our very simple approach reproduces fairly well the more detailed computations of Bird. Moreover it is apparent that for shorter periods our method will give better results in agreement with the theoretical expectation that for a homogeneous medium, that is, wavelength small against scale height, our method will be exact because it goes over into the simple wave theory.

Table 1. *Comparison of the heights of shock formation in* km *for two shock waves in a constant temperature gradient atmosphere computed with Eqs. (4) to (12) with computations of Bird (1964)*

Period (s)	Bird (Temp. gradient)	Bird (Uniform gas)	present work (Temp. gradient)
300	1100	1290	1265
150	600	640	664

3. Radiative Relaxation

a) Energy Equation

Neglecting viscous and thermal conduction losses the energy equation may be written (Hirschfelder *et al.*, 1964, p. 463)

$$\varrho c_v \left(\frac{\partial T}{\partial t} + v \frac{\partial T}{\partial x} \right) + p \frac{\partial v}{\partial x} = 4\pi\varrho (j - \bar{K} J) \tag{14}$$

Here j is the emission coefficient, J the mean intensity and $\bar{K}$ the Rosseland mean absorption coefficient, T the temperature and p the pressure of the gas element, c_v the specific heat at constant volume. Assuming that the radiation field is negligibly disturbed out of radiative equilibrium by the small perturbation T' where $T = T_0 + T'$ and assuming LTE we may write after linearization

$$\varrho c_v \frac{\partial T'}{\partial t} + p \frac{\partial v}{\partial x} = 16 \varrho \bar{K} \sigma T_0^3 T' \tag{15}$$

where T_0 is the temperature of the undisturbed atmosphere.

The radiative relaxation time is given by

$$T_R = \frac{c_v}{16\,\bar{K}\sigma T_0^3} \tag{16}$$

The relationship between temperature and velocity in a sound wave is given by

$$T' = T_0(\gamma - 1)\frac{v}{c} \tag{17}$$

where

$$c^2 = \gamma \frac{p}{\varrho} \tag{18}$$

With these relations Eq. (15) may be written

$$\left(\frac{1}{c}\frac{\partial}{\partial t} + \frac{\partial}{\partial x}\right) T' = \frac{dT'}{dx} = -\frac{T'}{T_R c}, \tag{19}$$

or integrated

$$T' = T'_0 e^{-\int_0^{\infty} \frac{dx}{T_R(x)c(x)}} \tag{20}$$

The physical meaning of Eq. (19) is that the high (or low) temperature region T' travelling with sound velocity suffers radiative loss proportional to the temperature perturbation T'. A more detailed derivation of Eq. (20) for the case of a stationary temperature perturbation has been given by Spiegel (1957).

b) Inclusion of Radiative Losses

The inclusion of radiative losses for the case of small amplitude may now easily be done using a pretabulated set of values

$$e(i) = e^{-\int_0^{x(i)} \frac{dx}{T_R(x)c(x)}} \tag{21}$$

where $x\,(i)$ is the height grid of Eq. (3).

Because of Eq. (17) and (21) we just need to follow up operation (4) by

$$\bar{v}_2(i) = v'_2(i)\, e(i+K)/e(i) \tag{22}$$

and continue with $\bar{v}_2(i)$ instead of $v'_2(i)$ in Eq. (6) to (12).

In Table 2 we have tabulated the radiative relaxation time T_R and the profile diminution function $e(i)$ as function of height on basis of the HRA model (Gingerich *et al.*, 1971). The opacity in Eq. (16) was computed using H^- and hydrogen absorption. For the H^- absorption the routine of Gingerich (1964) was taken multiplied by the non-LTE hydrogen number density. In the hydrogen absorption the LTE number density was used because the Balmer emission is not far out of LTE.

Table 2. *Radiative relaxation time T_R after Eq. (16) and profile diminution function e (i) after Eq. (21) as function of height on basis of the* HRA *model (Gingerich et al., 1971).*

h (km)	T_R (s)	e
—46.8	0.026	2.55×10^{21}
0	0.698	1
48.9	2.54	1.32×10^{-2}
108	6.03	1.91×10^{-3}
153	9.96	8.83×10^{-4}
198	15.4	5.39×10^{-4}
297	39.4	3.03×10^{-4}
393	99.6	2.42×10^{-4}
501	290	2.19×10^{-4}
606	652	2.12×10^{-4}
685	743	2.08×10^{-4}
797	471	2.03×10^{-4}
1022	365	1.89×10^{-4}
1288	288	1.74×10^{-4}

b) The Effect of Optical Depth

In Table 2 we see that the wave looses energy extremely rapid within the first 100 km. This is only partly realistic and results from our optically thin treatment of the radiation loss. A more detailed treatment taking into account the optical depth and the perturbation of the opacity and radiation field will greatly reduce the radiation loss rate.

However there is also some uncertainty at what height we might suppose the initial acoustical flux computed by Stein (1968) to be present. Because the acoustic emission rate is proportional to u^8 where u is the mean velocity of the rising turbulence element the greatest emission will come from the height of greatest u. This is according to Vitense (1953) at $\log p_g = 5.25$ or at -51 km in the Gingerich *et al.* (1971) model. The profile diminution factor $e\,(i)$ at that height (Table 2) shows dramatically the need for a better treatment of absorption.

To account for this missing absorption we have cut off in our approximate treatment the radiation loss arbitrarily at a certain height h_c for which we took between 110 to 140 km, below which we consider the atmosphere as completely optically thick and above which we treat the radiation loss according to Eq. (22). The above cut-off height h_c was chosen such that at 800 km still a total energy flux of about $1 \times 10^6 \frac{\text{erg}}{\text{cm}^2 s}$ is present, to be able to balance the observed chromospheric and coronal radiation losses.

4. The Acoustic Flux Spectrum

Stein (1968) has computed three acoustic flux spectra on basis of different assumptions on the space and frequency behaviour of the turbulence in the solar convection zone. He calls these spectra EE, SE and EG spectra. The EG spectrum will be disregarded in this work because it has an unrealistically low total flux. The total fluxes are for the EE spectrum $\pi F_{\text{tot}} = 7.7 \times 10^7$ erg/cm^2 s and for the SE spectrum $\pi F_{\text{tot}} = 5.5 \times 10^7$ erg/cm^2 s. (Note that the total flux of the EE spectrum is misprinted in Steins paper).

We want to represent this spectrum by a series of N monochromatic bands of bandwidth $\Delta\omega$. The total flux is then computed by

$$\pi F_{\text{tot}} = \int \pi F \, d\omega = \sum_{j=1}^{N} \pi F_{\omega_j} \Delta\omega = \sum_{j=1}^{N} \pi F_j \quad (23)$$

where $N\Delta\omega$ is the total bandwidth.

Increasing the number of partitions N we notice that because of the decrease of $\Delta\omega$ the fluxes πF_j decrease correspondingly. Using now Eq. (24)

$$\pi F_j = \varrho_0 c v_j^2 \quad (24)$$

to determine the wave amplitude v_j would be quite misleading.

The arbitrary splitting of the spectrum in monochromatic regions is perfectly valid in cases where linear effects are investigated. In our case however the formation of shocks which we want to consider is mainly a nonlinear effect. Thus it depends very critically on the wave amplitude and a procedure how to compute it has to be given on physical grounds.

The physical situation of wave production on the sun is a statistical process where wavetrains of acoustic waves are generated by the rising and falling turbulence elements. We expect a random spatial and temporal superposition of these wave trains in such a way as to yield the correct monochromatic flux by averaging over a sufficiently large area or a sufficiently long time interval Δt_A.

A simulation of a situation like that seems difficult even for a large computer. Thus a simplified physical picture is necessary. Thinking of the motion of the turbulence elements and their appearance in form of the granulation at the solar surface we may assume a very similar occurrence of acoustic wave trains. These may be pictured as pieces of monochromatic waves which appear at different surface elements and at different times. Considering a fixed surface element we assume thus that monochromatic wavetrains appear in time intervals $\Delta t_A/N$ where Δt_A is a sufficiently long time interval in which the complete flux spectrum can be measured at that surface element. N is the number of different monochromatic waves possible and thus identical with the number of frequencies in which we split the complete spectrum.

From Eq. (23) we get now the energy which has moved through the surface element in the averaging time Δt_A

$$\pi F_{\text{tot}} \Delta t_A = \sum_{j=1}^{N} N \pi F_j \frac{\Delta t_A}{N} . \quad (25)$$

The velocity amplitude is then simply computed using

$$N \pi F_j = \varrho_0 c v_j^2 . \quad (26)$$

5. Results and Discussion

a) Initial Conditions

The EE and SE energy flux spectra computed by Stein (1968) were split in 11 and 9 monochromatic frequency bands respectively. Tab. 3 shows the wave periods P_j and fluxes πF_j of these bands.

Table 3. *Wave periods P_j and fluxes πF_j of the monochromatic frequency bands j into which the* EE *and* SE *spectra were split.*

band	EE spectrum		SE spectrum	
j	P_j (s)	$\pi F_j \left(\frac{\text{erg}}{\text{cm}^2 s}\right)$	P_j (s)	$\pi F_j \left(\frac{\text{erg}}{\text{cm}_2 s}\right)$
1	251.3	1.52×10^6	125.7	2.72×10^6
2	83.8	8.90×10^6	41.9	1.09×10^7
3	50.3	1.59×10^7	25.1	1.25×10^7
4	35.9	1.69×10^7	18.0	9.70×10^6
5	27.9	1.33×10^7	14.0	6.68×10^6
6	22.9	9.24×10^6	11.4	4.36×10^6
7	19.3	5.47×10^6	9.67	2.76×10^6
8	16.8	2.67×10^6	8.38	1.69×10^6
9	14.8	1.17×10^6	7.39	1.13×10^6
10	13.2	5.00×10^5		
11	12.0	2.15×10^5		

To compute the behavior of a monochromatic wave we choose P_j, πF_j and the number of partitions I in regions of constant sound velocity for which we usually take 60 to 120. Using Eq. (26) we compute the wave amplitude v_j. At a chosen initial height h_c we appply the boundary condition

$$v(t) = v_j \sin\left(\frac{2\pi}{P_j} \Delta t (i-1)\right) \quad i = 1, \ldots, I+1 . \quad (27)$$

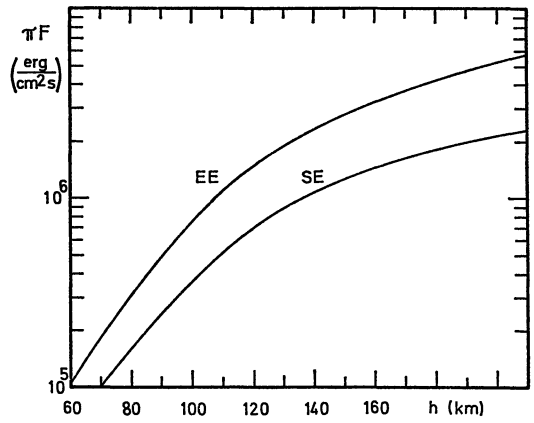

Fig. 2. Total flux of the acoustic wave spectra at the height 800 km as function of the cut-off height h_c

Using now Eqs. (4), (6) to (9), (11) and (22) and the HRA model (Gingerich *et al.*, 1971) as basis we compute the velocity amplitudes at the height points above h_c. Here

$$\Delta t = \frac{P_j}{I} . \tag{28}$$

A typical result of such a computation is seen in Fig. 3 where the velocity profile is plotted wherever the wave head reaches a multiple of 100 km.

Because of strong radiation losses at low altitude these wave amplitudes depend strongly on the cut-off height h_c below which we assume the atmosphere to be completely optically thick.

b) Dependence on Cut-off Height h_c

Fig. 2 shows the dependence of the total energy flux of the waves at a height of 800 km on the cut-off height h_c. As we have already mentioned we choose for our final computation the height h_c such that at 800 km a flux of about 1×10^6 erg/cm² s remains for the heating of the upper chromosphere and corona. Because the EE spectrum carries more total flux the cut-off height $h_c = 110$ km for this spectrum is lower than $h_c = 140$ km for the SE spectrum.

In these heights h_c all the uncertainties about the magnitude of the flux spectra resulting from our incomplete knowledge of the turbulent velocity field as well as the crudeness of our treatment of the optical depth effects are hidden. A more complete treatment should lower h_c to about 0 km. Because we have fixed the flux at 800 km in agreement with observations this uncertainty will not affect our results of the velocity profile.

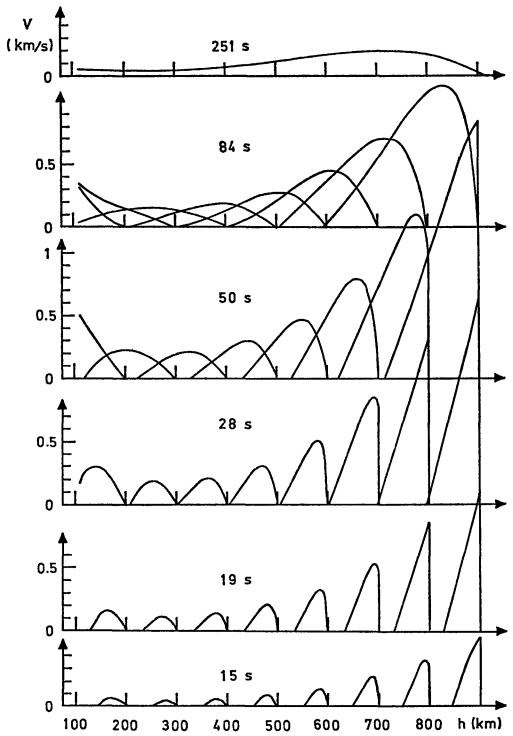

Fig. 3. Velocity amplitudes of monochromatic frequency bands of the EE spectrum versus height. Wave periods are indicated. Except for the wave with 250 s period the waves are drawn whenever the wave head reached a multiple of 100 km. The waves are introduced with a periodic boundary condition at $h_c = 110$ km

c) The Velocity Amplitudes

Figure 3 shows the velocity amplitudes of a few members of the monochromatic set of Tab. 3. The velocities are all plotted on the same scale. Because we have small amplitude waves, the positive and negative amplitudes are equal in magnitude. Thus the positive velocity pulses may be drawn analogously in the $-v$ direction. Here the shock front faces backwards.

At low altitude the strong damping of the waves because of the large radiative losses is apparent. At high altitude very little flux is lost by radiation and thus the waves are permitted to grow and develop into shock waves much earlier in spite of their small amplitude. This confirms the qualitative arguments of Ulmschneider (1971).

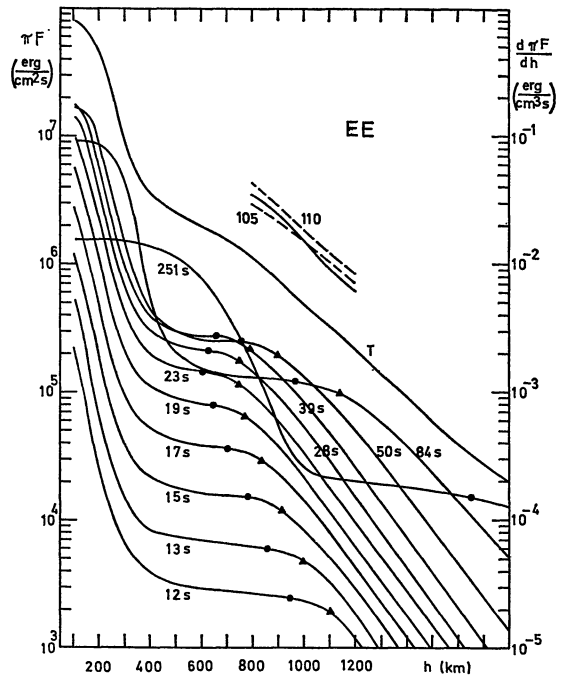

Fig. 4. Mechanical flux πF_j of the 11 monochromatic frequency bands of the EE spectrum as function of height. The total flux πF is labeled T. The heights at which shocks form and the shock is fully developed are indicated by dots and triangles respectively. The dissipation $\frac{d\pi F}{dh}$ (dashed, labeled by the heights h_c) is compared with computed radiation losses (drawn) between 800 and 1200 km

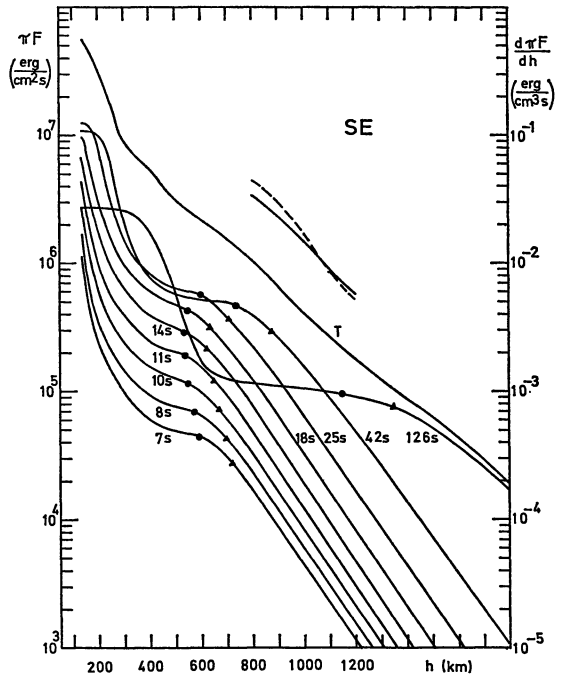

Fig. 5. Mechanical flux πF_j of the 9 monochromatic frequency bands of the SE spectrum as function of height. The total flux πF is labeled T. The heights at which shocks form and the shock is fully developed are indicated by dots and triangles respectively. The dissipation $\frac{d\pi F}{dh}$ (dashed) is compared with computed radiation losses (drawn) between 800 and 1200 km

d) The Monochromatic Fluxes

In Figs. 4 and 5 we have plotted the fluxes πF_j of the monochromatic frequency bands of the EE and SE spectra respectively as function of height. This flux was computed using Eqs. (1), (25) adding those parts of the wave which are below h_c. The strong decrease of the flux ($\sim v^2$) is seen here more predominantly. If there were no formation of shock waves these curves would level off at greater height after the radiative loss becomes unimportant. However as soon as a flux conservation condition is approached the wave grows rapidly because of the small scale height ($\sim$ 100 km) and nonlinear effects become important distorting the wave into a rapidly dissipating shock wave. The heights at which a shock discontinuity first appears are indicated by filled circles while the heights at which the shock wave is fully developed, when the velocity increases monotonically toward the shock front, are indicated by triangles. The total flux as function of height is indicated by the curve labeled T.

e) Mechanical Heating

The derivative of the total flux curve gives the dissipation. In Figs. 4 and 5 these mechanical dissipation rates (dashed) are compared with H^- and Balmer radiation loss rates (drawn, taken from Ulmschneider, 1971) between 800 and 1200 km. Radiative losses at these heights should be exactly balanced by mechanical heating. The remarkable agreement between the dissipation and radiation loss rates is apparent. The top curve in Fig. 4 labeled 110 gives the dissipation rate if h_c is 110 km. A lowering of h_c to 105 km yields the lower dissipation rate labeled 105 which shows how an appropriate choice of h_c will exactly balance dissipation and radiative loss.

f) General Picture of Chromospheric and Coronal Heating

Looking at the spectral composition of Figs. 4 and 5 we notice that regardless of the magnitude of the flux all high frequency waves develop into

shock waves at low heights. This supports strongly the picture already stated by Ulmschneider (1971) that the high frequency part of the acoustic spectrum is responsible for the heating of the chromosphere, It is also seen that the low frequency waves are the only remaining sources of energy for heights above 1800 km. Thus the coronal heating is done exclusively by waves of low frequency. Figures 3 and 4 show that at 800 km the main dissipator is the fully developed shock wave of 28 s period. This supports the previous findings based on an entirely monochromatic computation (Ulmschneider, 1970; 1971). However the present computation shows also that many waves participate in the heating of a certain height level. This is done in such a way that the frequency of the main dissipator decreases as function of height. Thus the heating of the chromosphere seems to be relatively well understood.

g) Corona

At 1800 km both frequency spectra yield a flux which is about a factor of 15 below the value needed for the balance of the Ly α and XUV emission which amounts to about 3×10^5 erg/cm^2 s (Ulmschneider, 1971). One reason for this low flux might be the inadequate treatment of the influence of optical depth on the radiation loss of low frequency waves. Spiegel (1957) shows that for long wavelength λ the radiative relaxation time T_R increases like

$$T_R\left(1-\frac{\bar{K}}{k}\cot^{-1}\frac{\bar{K}}{k}\right)^{-1}\approx 3\,T_R\left(\frac{\bar{K}}{k}\right)^2 \qquad (29)$$

where $k=2\pi/\lambda$ is the propagation vector and $\bar{K}$ the Rosseland mean opacity. Better treatment of this effect will greatly increase the flux carried by long period waves. Another possible reason could be magnetical energy generated at low heights. A third reason might be the neglect of gravity waves which Whitaker (1963) assumed to be the main heating agent of chromosphere and corona. The main objection against this view was the ready availability of acoustic waves and the severe influence of radiative relaxation on gravity waves. However a better treatment of these effects along with the gravity wave fluxes computed by Stein (1967) which are by a factor of about 10 higher than the acoustic wave flux might bring about the missing mechanical flux. Fourth a better treatment of the turbulence might yield an acoustic flux spectrum with greater power at long wavelength. Note that an uncertainty of the mean turbulent velocity u of a factor of 2 brings with the acoustic emission rate $\sim u^8$ a flux uncertainty of a factor of 256.

h) EE *versus* SE *Spectrum*

Finally we want to discuss the question of how well suited the EE and SE spectra are for chromospheric and coronal heating. Figures 4 and 5 show about the same flux at 800 km. Both spectra exhibit in addition good agreement of dissipation and radiation losses between 800 and 1200 km. In view of the fact however that both spectra are set up to have the same flux at 800 km this good agreement does not surprise. Thus before a better treatment of the optical depth is available we can not decide whether the EE or SE spectrum fits observation better. In order to bring more flux to great altitude however we would prefer a spectrum with a greater low frequency power.

Note added in Proof (29 July 1971). Two further points show the surprising consistency of our results with expectation. First the height at which the first member of the frequency band develops into a shock wave and thus starts to dissipate agrees very well with the height of the observed solar temperature minimum as seen in Figs. 4 and 5. Second the cut-off heights h_c of the SE and EE spectra lie at an optical depth of $\tau_{5000}=0.1$ to 0.2. This is exactly what one expects for the effect of the optical depth on radiative relaxation (see Section 3c).

Literature

Bird, G.A. 1964, *Ap. J.* **140**, 288.
Gingerich, O. 1964, *Smithson. astrophys. Obs. Spec, Rep.* **167**, 17.
Gingerich, O., Noyes, R.Wi, Kalkofen, W., Cuny, Y. 1971, Harvard Smithsonian Reference Atmosphere, to be published.
Landau, L.D., Lifshitz, E.M. 1959, Fluid Mechanics, Pergamon, London.
Spiegel, E.A. 1957, *Ap. J.* **126**, 202.
Stein, R.F. 1967, *Solar Phys.* **2**, 385.
1968, *Ap. J.* **154**, 297.
Ulmschneider, P. 1970, *Solar Phys.* **12**, 403.
Ulmschneider, P. 1971, *Astr. Astrophys.* **12**, 297.
Vitense, E. 1953, *Z. Astrophys.* **32**, 135.

P. Ulmschneider
Astronomisches Institut und
Sternwarte Würzburg
Büttnerstraße 72
BRD-8700 Würzburg, Germany